

Sensing Accuracy Optimization for Communication-assisted Dual-baseline UAV-InSAR

Mohamed-Amine Lahmeri*, Víctor Mustieles-Pérez*[†], Martin Vossiek*, Gerhard Krieger*[†],
and Robert Schober*

*Friedrich-Alexander-Universität Erlangen-Nürnberg (FAU), Germany

[†]German Aerospace Center (DLR), Microwaves and Radar Institute, Weßling, Germany

Abstract

In this paper, we study the optimization of the sensing accuracy of unmanned aerial vehicle (UAV)-based dual-baseline interferometric synthetic aperture radar (InSAR) systems. A swarm of three UAV-synthetic aperture radar (SAR) systems is deployed to image an area of interest from different angles, enabling the creation of two independent digital elevation models (DEMs). To reduce the InSAR sensing error, i.e., the height estimation error, the two DEMs are fused based on weighted average techniques into one final DEM. The heavy computations required for this process are performed on the ground. To this end, the radar data is offloaded in real time via a frequency division multiple access (FDMA) air-to-ground backhaul link. In this work, we focus on improving the sensing accuracy by minimizing the worst-case height estimation error of the final DEM. To this end, the UAV formation and the power allocated for offloading are jointly optimized based on alternating optimization (AO), while meeting practical InSAR sensing and communication constraints. Our simulation results demonstrate that the proposed solution can improve the sensing accuracy by over 39% compared to a classical single-baseline UAV-InSAR system and by more than 12% compared to other benchmark schemes.

I. INTRODUCTION

The use of unmanned aerial vehicle (UAV) swarms for remote sensing has recently gained attention due to their flexibility and efficiency in data collection tasks [1]. This has led to an increased use of drones in diverse applications, such as mapping, monitoring traffic, and addressing climate change [2]. For these tasks, a variety of sensors can be deployed onboard, including cameras, LiDARs, and radars. In particular, the deployment of synthetic aperture radar (SAR) on UAVs has attracted significant interest due to its ability to provide very high-resolution SAR images over local areas, even under challenging conditions,

This work was supported in part by the Deutsche Forschungsgemeinschaft (DFG, German Research Foundation) GRK 2680 – Project-ID 437847244.

overcoming the limitations of traditional airborne and spaceborne systems. This integration has sparked multiple recent studies focusing on system design [3], trajectory and resource allocation optimization [4]–[6], and experimental measurement campaigns for UAV-SAR systems [7].

An interesting remote sensing application of UAV swarms is three-dimensional (3D) radar imaging, which can be realized using techniques, such as multiple-input multiple-output (MIMO) radar, tomography, and interferometry [8]. In particular, interferometric synthetic aperture radar (InSAR) leverages the phase differences between at least two SAR images, captured from different angles, to extract topographic information and generate digital elevation models (DEMs). Key performance metrics in interferometry include signal-to-noise ratio (SNR), coverage, coherence, height of ambiguity (HoA), and height error [9], [10], which are affected by the interferometric baseline, i.e., the distance between the sensing platforms. While InSAR has been extensively studied for spaceborne and airborne platforms [8], the optimization of InSAR performance for UAV-based systems remains largely unexplored. In our recent research work [11], we investigated formation and resource allocation optimization for maximizing the InSAR coverage, but for a single-baseline UAV-InSAR system. In contrast, dual-baseline InSAR systems offer advantages, such as enhanced phase unwrapping and improved sensing accuracy [12]. However, results from single-baseline systems [11] do not apply to dual-baseline systems due to the different expressions for the height error and the use of multiple acquisition geometries.

In this work, we study a dual-baseline UAV-based InSAR system, where a swarm consisting of one master and two slave UAVs is deployed to generate two independent DEMs of a target area, which are then fused into a single DEM based on weighted averaging [12]. Additionally, the radar data is offloaded to the ground in real time. We investigate the joint optimization of the UAV formation and communication power allocation for minimization of the worst-case height error in the final DEM under communication and sensing constraints. Our main contributions can be summarized as follows:

- We propose an approximate bi-static SNR expression valid for the considered sensing application.
- Based on the Cramér–Rao bound of the phase error, we derive a tractable upper bound for the complex expression of the height error of the final DEM.
- We formulate and solve a joint optimization problem for UAV formation and communication power allocation to minimize the derived upper bound on the height error, while satisfying sensing and communication constraints.
- Our simulation results demonstrate the effectiveness of the considered dual-baseline InSAR system compared to single-baseline systems and other benchmark schemes.

Notations: In this paper, lower-case letters x refer to scalar variables, while boldface lower-case letters

\mathbf{x} denote vectors. $\{a, \dots, b\}$ denotes the set of all integers between a and b . $|\cdot|$ denotes the absolute value operator. \mathbb{R}^N represents the set of all N -dimensional vectors with real-valued entries. For a vector $\mathbf{x} = (x_1, \dots, x_N)^T \in \mathbb{R}^N$, $\|\mathbf{x}\|_2$ denotes the Euclidean norm, whereas \mathbf{x}^T stands for the transpose of \mathbf{x} . For real-valued multivariate functions $f(\mathbf{x})$, $\frac{\partial f}{\partial \mathbf{x}}(\mathbf{a}) = \left(\frac{\partial f}{\partial x_1}(\mathbf{a}), \dots, \frac{\partial f}{\partial x_N}(\mathbf{a}) \right)^T$ denotes the partial derivative of f with respect to (w.r.t.) \mathbf{x} evaluated for an arbitrary vector \mathbf{a} . For any Boolean expression \mathcal{S} , $1\{\mathcal{S}\}$ denotes the indicator function, which equals 1 if \mathcal{S} is true and 0 otherwise.

II. SYSTEM MODEL

We consider three rotary-wing UAVs, denoted by $U_k, k \in \{0, 1, 2\}$, performing InSAR sensing over a target area. U_0 , the master drone, transmits and receives radar echoes, while U_1 and U_2 , the slave drones, only receive. We use a 3D coordinate system, where the x -, y -, and z -axes represent the range direction, the azimuth direction, and the altitude, respectively. The mission time T is divided into N slots of duration δ_t , with $T = N \cdot \delta_t$. The drone swarm forms a dual-baseline interferometer with two independent observations acquired by (U_0, U_1) and (U_0, U_2) , respectively. The considered UAV-SAR systems operate in stripmap mode [13] and fly at a constant velocity, v_y , following a linear trajectory that is parallel to a line, denoted by l_t , which is parallel to the y -axis and passes in time slot n through reference point $\mathbf{p}_t[n] = (x_t, y[n], 0)^T \in \mathbb{R}^3$, see Figure 1. The position of U_k in time slot $n \in \{1, \dots, N\}$ is $\mathbf{q}_k[n] = (x_k, y[n], z_k)^T$, with the y -axis position vector $\mathbf{y} = (y[1] = 0, y[2], \dots, y[N])^T \in \mathbb{R}^N$ given by:

$$y[n+1] = y[n] + v_y \delta_t, \forall n \in \{1, N-1\}. \quad (1)$$

For simplicity, we denote the position of U_k in the across-track plane (i.e., xz -plane) by $\mathbf{q}_k = (x_k, z_k)^T \in \mathbb{R}^2, \forall k \in \{0, 1, 2\}$. The interferometric baseline, b_k , which refers to the distance between sensors U_0 and U_k , is given by:

$$b_k(\mathbf{q}_0, \mathbf{q}_k) = \|\mathbf{q}_k - \mathbf{q}_0\|_2, \forall k \in \{1, 2\}. \quad (2)$$

The perpendicular baseline, denoted by $b_{\perp,k}$, is the magnitude of the projection of U_k 's baseline vector perpendicular to U_0 's line-of-sight (LOS) to $\mathbf{p}_t[n]$ and is given by:

$$b_{\perp,k}(\mathbf{q}_0, \mathbf{q}_k) = b_k(\mathbf{q}_0, \mathbf{q}_k) \cos\left(\theta_0 - \alpha_k(\mathbf{q}_0, \mathbf{q}_k)\right), \forall k \in \{1, 2\}, \quad (3)$$

where θ_0 is the fixed look angle that U_0 's LOS has with the vertical, and α_k is the angle between the interferometric baseline b_k and the horizontal plane.

A. InSAR Performance

Next, we introduce the relevant InSAR sensing performance metrics.

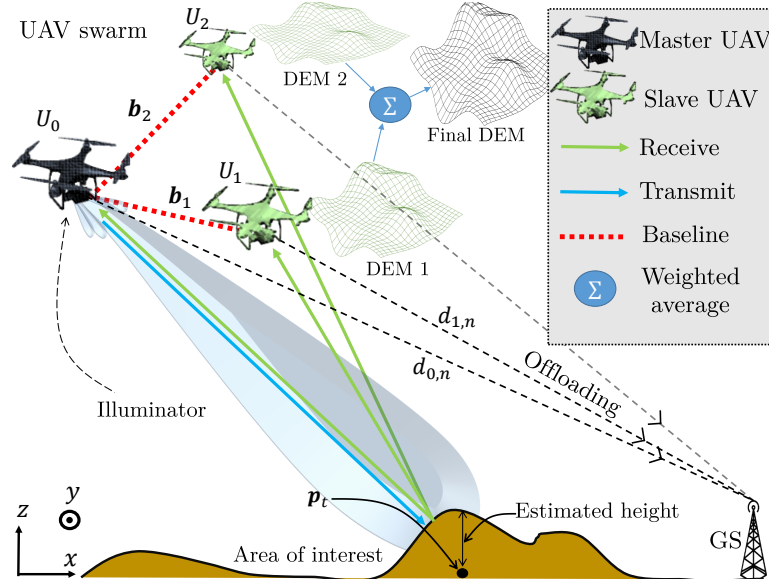


Fig. 1: Dual-baseline InSAR sensing system comprising one master and two slave UAV-SAR systems as well as a ground station (GS) for real-time data offloading.

1) *InSAR Coverage*: Let $r_k, k \in \{0, 1, 2\}$, denote U_k 's slant range w.r.t. $\mathbf{p}_t[n]$. The slant range is independent of time and is given by:

$$r_k(\mathbf{q}_k) = \sqrt{(x_k - x_t)^2 + z_k^2}, \forall k \in \{0, 1, 2\}. \quad (4)$$

The radar swath is designed to be centered w.r.t. l_t . To this end, the look angle of the slave UAVs, denoted by $\theta_k(\mathbf{q}_k), k \in \{1, 2\}$, is adjusted such that the beam footprint is centered around \mathbf{p}_t , i.e., $\theta_k(\mathbf{q}_k) = \arctan\left(\frac{x_k - x_t}{z_k}\right)$. The swath width of U_k can be approximated as follows [13]:

$$S_k(\mathbf{q}_k) = \frac{\Theta_{3\text{dB}} r_k(\mathbf{q}_k)}{\cos(\theta_k(\mathbf{q}_k))}, \forall k \in \{0, 1, 2\}, \quad (5)$$

where $\Theta_{3\text{dB}}$ is the -3 dB beamwidth in elevation.

2) *InSAR Coherence*: A key performance metric for InSAR is coherence, representing the cross-correlation between two SAR images. For the images acquired by $(U_0, U_k), k \in \{1, 2\}$, the total coherence can be decomposed into several decorrelation sources as follows:

$$\gamma_k(\mathbf{q}_0, \mathbf{q}_k) = \gamma_{\text{Rg},k}(\mathbf{q}_k) \gamma_{\text{SNR},k}(\mathbf{q}_0, \mathbf{q}_k) \gamma_{\text{other}}, \forall k \in \{1, 2\}, \quad (6)$$

where $\gamma_{\text{Rg},k}$ is the baseline decorrelation, $\gamma_{\text{SNR},k}$ is the SNR decorrelation, and γ_{other} represents the contribution from all other decorrelation sources. The SNR decorrelation of pair (U_0, U_k) is affected by the

SNRs of both UAVs and is given by [10]:

$$\gamma_{\text{SNR},k}(\mathbf{q}_0, \mathbf{q}_k) = \frac{1}{\sqrt{1 + \text{SNR}_0^{-1}(\mathbf{q}_0)}} \frac{1}{\sqrt{1 + \text{SNR}_k^{-1}(\mathbf{q}_0, \mathbf{q}_k)}}, \quad (7)$$

where SNR_0 denotes the SNR of the mono-static acquisition by U_0 given by [10]:

$$\text{SNR}_0(\mathbf{q}_0) = \frac{\gamma_m}{r_0^3(\mathbf{q}_0)}, \quad (8)$$

where $\gamma_m = \frac{\sigma_0 P_t G_t G_r \lambda^3 c \tau_p \text{PRF}}{4^4 \pi^3 v_y \sin(\theta_0) k_b T_{\text{sys}} B_{\text{Rg}} F L}$. Here, σ_0 is the normalized backscatter coefficient, P_t is the radar transmit power, G_t and G_r are the transmit and receive antenna gains, respectively, λ is the radar wavelength, c is the speed of light, τ_p is the pulse duration, PRF is the pulse repetition frequency, k_b is the Boltzmann constant, T_{sys} is the receiver temperature, B_{Rg} is the bandwidth of the radar pulse, F is the noise figure, and L represents the total radar losses. The derivation of the bi-static SNR for U_k , denoted by SNR_k , is more complicated. Here, assuming a small bi-static angle $|\theta_0 - \theta_k|$, which holds for InSAR applications [8], we propose the following approximation¹:

$$\text{SNR}_k(\mathbf{q}_0, \mathbf{q}_k) \approx \frac{\gamma_m}{r_0^2(\mathbf{q}_0) r_k(\mathbf{q}_k)}, \forall k \in \{1, 2\}. \quad (9)$$

Furthermore, the baseline decorrelation reflects the loss of coherence caused by the different angles used for the acquisition of both InSAR images [14]:

$$\gamma_{\text{Rg},k}(\mathbf{q}_k) = \frac{1}{B_p} \left[\frac{2 + B_p}{1 + \mathcal{X}(\mathbf{q}_k)} - \frac{2 - B_p}{1 + \mathcal{X}^{-1}(\mathbf{q}_k)} \right], \quad (10)$$

where $B_p = \frac{B_{\text{Rg}}}{f_0}$ is the fractional bandwidth, f_0 is the radar center frequency, and function \mathcal{X} is given by [14]:

$$\mathcal{X}(\mathbf{q}_k) = \frac{2 \left(\sin(\theta_0) \mathbb{1}\{\theta_0 > \theta_k(\mathbf{q}_k)\} + \sin(\theta_k(\mathbf{q}_k)) \mathbb{1}\{\theta_0 \leq \theta_k(\mathbf{q}_k)\} \right)}{\sin(\theta_0) + \sin(\theta_k(\mathbf{q}_k))}. \quad (11)$$

3) *Height of Ambiguity (HoA)*: The HoA is related to the sensitivity of the radar system to topographic height variations [10]. The HoA of pair (U_0, U_k) is given by [10]:

$$h_{\text{amb},k}(\mathbf{q}_0, \mathbf{q}_k) = \frac{\lambda r_0(\mathbf{q}_0) \sin(\theta_0)}{b_{\perp,k}(\mathbf{q}_0, \mathbf{q}_k)}, \forall k \in \{1, 2\}. \quad (12)$$

¹Please find a detailed derivation of the approximated bi-static SNR expression in Appendix A.

4) *DEM Height Accuracy*: The height error of the DEM acquired by the InSAR pair (U_0, U_k) is given by [10]:

$$\sigma_{h_k}(\mathbf{q}_0, \mathbf{q}_k) = h_{\text{amb},k}(\mathbf{q}_0, \mathbf{q}_k) \frac{\sigma_{\Phi_k}(\mathbf{q}_0, \mathbf{q}_k)}{2\pi}, \forall k \in \{1, 2\}, \quad (13)$$

where σ_{Φ_k} is the random error in the interferometric phase and can be approximated in the case of high interferometric coherences by the Cramér–Rao bound [8]:

$$\sigma_{\Phi_k}(\mathbf{q}_0, \mathbf{q}_k) = \frac{1}{\gamma_k(\mathbf{q}_0, \mathbf{q}_k)} \sqrt{\frac{1 - \gamma_k^2(\mathbf{q}_0, \mathbf{q}_k)}{2n_L}}, \forall k \in \{1, 2\}, \quad (14)$$

where n_L is the number of independent looks employed, i.e., n_L adjacent pixels of the interferogram are averaged to improve phase estimation [8]. The fusion of the two independent InSAR DEMs is performed based on inverse-variance weighting, such that the height of an arbitrary target estimated by InSAR pair (U_0, U_k) , denoted by h_k , is weighted by $w_k(\mathbf{q}_0, \mathbf{q}_k) = \frac{1}{\sigma_{h_k}^2(\mathbf{q}_0, \mathbf{q}_k)}$, $k \in \{1, 2\}$, and averaged as $\frac{h_1 w_1 + h_2 w_2}{w_1 + w_2}$. The final height error of the fused DEM is characterized by [12]:

$$\sigma_h(\mathbf{q}_0, \mathbf{q}_1, \mathbf{q}_2) = \sqrt{\frac{\sum_{k \in \{1,2\}} w_k^2(\mathbf{q}_0, \mathbf{q}_k) \sigma_{h_k}^2(\mathbf{q}_0, \mathbf{q}_k)}{\left(\sum_{k \in \{1,2\}} w_k(\mathbf{q}_0, \mathbf{q}_k) \right)^2}}. \quad (15)$$

B. Communication Performance

We consider real-time offloading of the radar data to a GS, where the master and slave UAVs employ frequency-division multiple-access (FDMA). The instantaneous communication transmit power consumed by UAV U_k is given by $\mathbf{P}_{\text{com},k} = (P_{\text{com},k}[1], \dots, P_{\text{com},k}[N])^T \in \mathbb{R}^N$, $k \in \{0, 1, 2\}$. We denote the location of the GS by $\mathbf{g} = (g_x, g_y, g_z)^T \in \mathbb{R}^3$ and the distance from U_k to the GS by $d_{k,n}(\mathbf{q}_k) = \|\mathbf{q}_k[n] - \mathbf{g}\|_2$, $\forall k \in \{0, 1, 2\}, \forall n$. Thus, adopting the free-space path loss model and FDMA, the instantaneous throughput from U_k , $\forall k \in \{0, 1, 2\}$, to the GS is given by:

$$R_{k,n}(\mathbf{q}_k, \mathbf{P}_{\text{com},k}) = B_{c,k} \log_2 \left(1 + \frac{P_{\text{com},k}[n] \beta_{c,k}}{d_{k,n}^2(\mathbf{q}_k)} \right), \forall n, \quad (16)$$

where $B_{c,k}$ is U_k 's fixed communication bandwidth and $\beta_{c,k}$ is the reference channel gain² divided by the noise variance.

²The reference channel gain is the channel power gain at a reference distance of 1 m.

III. PROBLEM FORMULATION

In this paper, we aim to minimize the height error of the final DEM σ_h by jointly optimizing the UAV formation $\mathcal{Q} = \{\mathbf{q}_k, \forall k \in \{0, 1, 2\}\}$ and the instantaneous communication transmit powers $\mathcal{P} = \{\mathbf{P}_{\text{com},k}, \forall k \in \{0, 1, 2\}\}$, while satisfying communication and sensing quality-of-service constraints. To this end, we formulate the following optimization problem:

$$\begin{aligned}
\text{(P)} : & \min_{\mathcal{Q}, \mathcal{P}} \sigma_h(\mathcal{Q}) \\
\text{s.t.} \quad & \text{C1} : z_{\min} \leq z_k \leq z_{\max}, \forall k \in \{0, 1, 2\}, \\
& \text{C2} : x_0 = x_t - z_0 \tan(\theta_0), \\
& \text{C3} : \theta_{\min} \leq \theta_k(\mathbf{q}_k) \leq \theta_{\max}, \forall k \in \{1, 2\}, \\
& \text{C4} : \|\mathbf{q}_i - \mathbf{q}_j\|_2 \geq d_{\min}, \forall i \neq j \in \{0, 1, 2\}, \\
& \text{C5} : S_k(\mathbf{q}_k) \geq S_{\min}, \forall k \in \{0, 1, 2\}, \\
& \text{C6} : \gamma_{\text{SNR},k}(\mathbf{q}_0, \mathbf{q}_k) \geq \gamma_{\text{SNR}}^{\min}, \forall k \in \{1, 2\}, \\
& \text{C7} : \gamma_{\text{Rg},k}(\mathbf{q}_k) \geq \gamma_{\text{Rg}}^{\min}, \forall k \in \{1, 2\}, \\
& \text{C8} : h_{\text{amb},k}(\mathbf{q}_0, \mathbf{q}_k) \geq h_{\text{amb}}^{\min}, \forall k \in \{1, 2\}, \\
& \text{C9} : 0 \leq P_{\text{com},k}[n] \leq P_{\text{com}}^{\max}, \forall k \in \{0, 1, 2\}, \forall n, \\
& \text{C10} : R_{k,n}(\mathbf{q}_k, \mathbf{P}_{\text{com},k}) \geq R_{\min,k}, \forall k \in \{0, 1, 2\}, \forall n, \\
& \text{C11} : \sum_{n=1}^N P_{\text{com},k}[n] \leq E_{\text{com}}^{\max}, \forall k \in \{0, 1, 2\}.
\end{aligned}$$

Constraint C1 specifies the maximum and minimum allowed flying altitude, denoted by z_{\max} and z_{\min} , respectively. Constraint C2 ensures that the beam footprint of the master UAV is centered around $\mathbf{p}_t[n]$. Constraint C3 specifies the minimum and maximum slave look angle, denoted by θ_{\min} and θ_{\max} , respectively. Constraint C4 ensures a minimum safety distance d_{\min} between any two UAVs. Constraint C5 imposes a minimum radar swath width S_{\min} . Constraints C6 and C7 ensure minimum thresholds for SNR and baseline decorrelation, $\gamma_{\text{SNR}}^{\min}$ and $\gamma_{\text{Rg}}^{\min}$, respectively. Constraint C8 imposes a minimum HoA, h_{amb}^{\min} , required for phase unwrapping [9]. Constraint C9 imposes a maximum communication transmit power, P_{com}^{\max} . Constraint C10 ensures the minimum required sensing data rate for U_k , $R_{\min,k}, \forall k \in \{0, 1, 2\}$. Constraint C11 limits the total communication energy of U_k to $E_{\text{com}}^{\max}, \forall k \in \{0, 1, 2\}$.

Problem (P) is a non-convex optimization problem. The non-convexity is caused by the objective function and constraints C4, C5, C7, and C8. In fact, the height error is simultaneously HoA- and coherence-

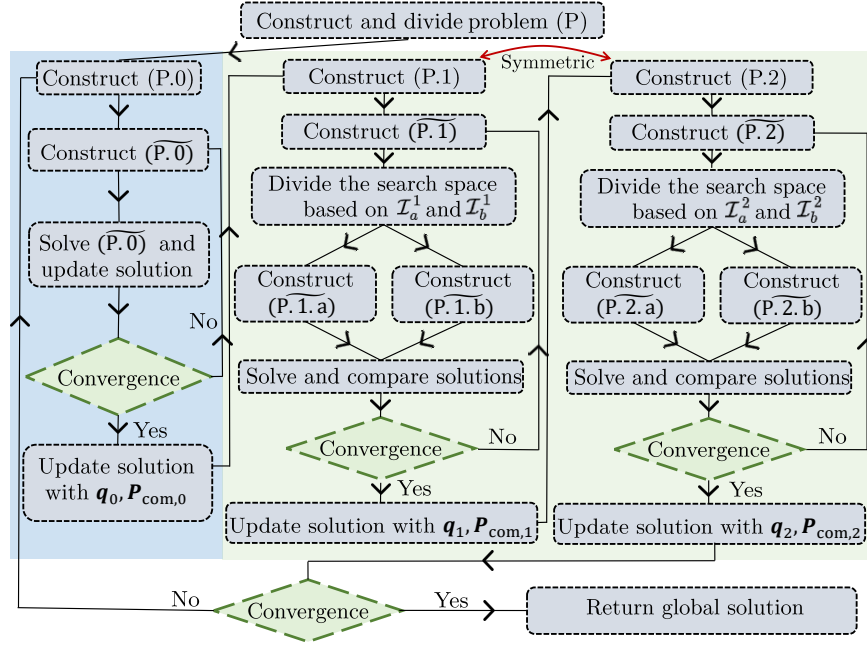


Fig. 2: Block diagram of the proposed solution to problem (P) given by alternating optimization (AO)-based **Algorithm 2**.

dependent, making the objective function challenging. Moreover, the lower bound on an Euclidean distance in C4 and the trigonometric functions in C5, C7, and C8 make these constraints non-convex and difficult to handle.

IV. SOLUTION OF THE OPTIMIZATION PROBLEM

To balance performance and complexity, we propose a low-complexity sub-optimal solution that minimizes an upper bound on problem (P) based on AO. We divide problem (P) into 3 sub-problems: (P.0), (P.1), and (P.2). In (P.0), we optimize the position and communication power of U_0 , whereas in (P.1) and (P.2), we optimize the positions and communication powers of U_1 and U_2 , respectively. Due to symmetry, we focus on (P.0) and (P.1), as (P.2) can be solved similarly to (P.1), see Figure 2.

A. Master UAV Optimization

In this sub-section, we optimize the position and communication transmit power of the master UAV, denoted by \mathbf{q}_0 and $\mathbf{P}_{\text{com},0}$, respectively, for fixed $\{\mathbf{q}_1, \mathbf{q}_2, \mathbf{P}_{\text{com},1}, \mathbf{P}_{\text{com},2}\}$. The resulting sub-problem, denoted by (P.0), is still non-convex due to its objective function and C4. Yet, we leverage successive

convex approximation (SCA) to provide a low-complexity solution for (P.0).

As the master look angle θ_0 is fixed, the perpendicular baseline is independent of \mathbf{q}_0 and is given by [11]:

$$b_{\perp,k}(\mathbf{q}_k) = \frac{|(x_t - x_k) - \tan(\theta_0)z_k|}{\sqrt{\tan(\theta_0)^2 + 1}}, \forall k \in \{1, 2\}. \quad (17)$$

Proposition 1. *The height error of the final DEM, σ_h , can be upper bounded based on the worst-case coherence as follows:*

$$\sigma_h(\mathcal{Q}) \leq \overline{\sigma}_h(\mathcal{Q}) \triangleq \sqrt{\frac{\lambda^2 r_0^2(\mathbf{q}_0) \sin^2(\theta_0)(1 - \mathcal{A}^2)}{8\pi^2 \mathcal{A}^2 n_L (b_{\perp,1}^2(\mathbf{q}_1) + b_{\perp,2}^2(\mathbf{q}_2))}}, \quad (18)$$

where $\mathcal{A} = \gamma_{\text{Rg}}^{\min} \gamma_{\text{SNR}}^{\min} \gamma_{\text{other}}$.

Proof. Please refer to Appendix B. □

Therefore, we relax the complex objective function of (P.0) by minimizing instead the upper bound on the height error, denoted by $\overline{\sigma}_h$ and provided in **Proposition 1**. In iteration i of the SCA algorithm, constraint C4 is tackled using a surrogate function for the Euclidean distance $\|\mathbf{q}_0 - \mathbf{q}_k\|_2$ around $\mathbf{q}_0^{(i)}$ as follows [15]:

$$\widetilde{\text{C4}} : 2\mathbf{q}_0^T(\mathbf{q}_0^{(i)} - \mathbf{q}_k) - \|\mathbf{q}_0^{(i)}\|_2^2 + \|\mathbf{q}_k\|_2^2 \geq d_{\min}, \forall i, \forall k \in \{1, 2\}. \quad (19)$$

The resulting sub-problem is denoted by $(\widetilde{\text{P.0}})$ and is given by:

$$\begin{aligned} (\widetilde{\text{P.0}}) : \quad & \min_{\mathbf{q}_0, \mathbf{P}_{\text{com},0}} \overline{\sigma}_h(\mathcal{Q}) \\ \text{s.t.} \quad & \text{C1} - \text{C3}, \widetilde{\text{C4}}, \text{C5}, \text{C6}, \text{C8} - \text{C11}. \end{aligned}$$

Problem $(\widetilde{\text{P.0}})$ is convex and can be solved using the Python CVXPY library [16]. The solution procedure to solve (P.0) is summarized in **Algorithm 1**, which converges to a local optimum of the upper bound on problem (P.0), $\overline{\sigma}_h$, in polynomial computational time complexity [17]. **Algorithm 1** involves $N + 2$ optimization variables, resulting in a computational complexity of $\mathcal{O}(M_0(N + 2)^{3.5})$, where M_0 is the number of iterations needed for convergence [17].

B. Slave UAV Optimization

Next, we optimize the position and communication transmit power of slave UAV U_1 , denoted by \mathbf{q}_1 and $\mathbf{P}_{\text{com},1}$, respectively, for fixed $\{\mathbf{q}_0, \mathbf{q}_2, \mathbf{P}_{\text{com},0}, \mathbf{P}_{\text{com},2}\}$. The resulting problem, denoted by (P.1), is non-convex due to the objective function and constraints C4, C5, C7, and C8. To tackle this sub-problem, we employ again SCA. First, we adopt the upper bound $\overline{\sigma}_h$ provided by **Proposition 1**. Furthermore, it can be shown that minimizing $\overline{\sigma}_h$ for fixed \mathbf{q}_0 and \mathbf{q}_2 is equivalent to maximizing the perpendicular baseline

Algorithm 1 Successive Convex Approximation Algorithm

- 1: For fixed $\{\mathbf{q}_1, \mathbf{q}_2, \mathbf{P}_{\text{com},1}, \mathbf{P}_{\text{com},2}\}$, set initial point $\mathbf{q}_0^{(1)}$, iteration index $i = 1$, and error tolerance $0 < \epsilon_0 \ll 1$.
 - 2: **repeat**
 - 3: Determine sensing worst-case accuracy $\overline{\sigma}_h(\mathbf{q}_0, \mathbf{q}_1, \mathbf{q}_2)$, \mathbf{q}_0 , and $\mathbf{P}_{\text{com},0}$ by solving $(\widetilde{\text{P.0}})$ around point $\mathbf{q}_0^{(i)}$ using
 CVXPY
 - 4: Set $i = i + 1$ and $\mathbf{q}_0^{(i)} = \mathbf{q}_0$
 - 5: **until** $\left| \frac{\overline{\sigma}_h(\mathbf{q}_0^{(i)}, \mathbf{q}_1, \mathbf{q}_2) - \overline{\sigma}_h(\mathbf{q}_0^{(i-1)}, \mathbf{q}_1, \mathbf{q}_2)}{\overline{\sigma}_h(\mathbf{q}_0^{(i)}, \mathbf{q}_1, \mathbf{q}_2)} \right| < \epsilon_0$
 - 6: **return** solution $\{\mathbf{q}_0, \mathbf{P}_{\text{com},0}\}$
-

$b_{\perp,1}(\mathbf{q}_1)$. Moreover, in each SCA iteration j , non-convex constraint C4 is replaced with convex constraint $\widetilde{\text{C4}}$ based on a surrogate function similar to (19). Constraint C5 is convexified based on a Taylor approximation around point $\mathbf{q}_1^{(j)}$ as follows:

$$\widetilde{\text{C5}} : r_1^2(\mathbf{q}_1^{(j)}) + \left(\frac{\partial r_1^2}{\partial \mathbf{q}_1}(\mathbf{q}_1^{(j)}) \right)^T (\mathbf{q}_1 - \mathbf{q}_1^{(j)}) \geq \frac{S_{\min} z_1}{\Theta_{3\text{dB}}}, \forall j. \quad (20)$$

The resulting problem is given by:

$$\begin{aligned} (\widetilde{\text{P.1}}) : \quad & \max_{\mathbf{q}_1, \mathbf{P}_{\text{com},1}} b_{\perp,1}(\mathbf{q}_1) \\ \text{s.t.} \quad & \text{C1, C3, } \widetilde{\text{C4}}, \widetilde{\text{C5}}, \text{C6} - \text{C11}. \end{aligned}$$

Yet, the expressions for the perpendicular baseline in (17) and for the baseline decorrelation still present obstacles for solving $(\widetilde{\text{P.1}})$. Thus, we divide the search space of problem $(\widetilde{\text{P.1}})$ into two disjoint sets, denoted by $\mathcal{I}_a^k = \{\mathbf{q}_k; \theta_0 \geq \theta_k(\mathbf{q}_k)\}$ and $\mathcal{I}_b^k = \{\mathbf{q}_k; \theta_0 < \theta_k(\mathbf{q}_k)\}$, $k \in \{1, 2\}$. The solution that maximizes $\overline{\sigma}_h$ over \mathcal{I}_a^1 and \mathcal{I}_b^1 is selected, see Figure 2.

Proposition 2. *Constraint C7 is equivalent to the following convex constraints:*

$$\begin{cases} \text{C7a} : z_k \alpha_a - (x_t - x_k) \leq 0, & \text{if } \mathbf{q}_k \in \mathcal{I}_a^k \\ \text{C7b} : (x_t - x_k) - z_k \alpha_b \leq 0, & \text{if } \mathbf{q}_k \in \mathcal{I}_b^k \end{cases}, \forall k \in \{1, 2\}, \quad (21)$$

where $\alpha_a = \tan \left(\arcsin \left(\frac{2-h(\gamma_{\text{Rg}}^{\min})}{h(\gamma_{\text{Rg}}^{\min})} \sin(\theta_0) \right) \right)$, $\alpha_b = \tan \left(\arcsin \left(\frac{h(\gamma_{\text{Rg}}^{\min})}{2-h(\gamma_{\text{Rg}}^{\min})} \sin(\theta_0) \right) \right)$, and function $h(x) = \frac{x B_p - 2 - B_p}{B_p - 2 - x B_p}$.

Proof. Please refer to Appendix C. □

Constraint C7 is transformed based on **Proposition 2**. Then, for $\mathbf{q}_1 \in \mathcal{I}_a^1$, constraint C7 is replaced by C7a and the resulting problem is denoted by $\widetilde{\text{(P.1.a)}}$. Similarly, sub-problem $\widetilde{\text{(P.1.b)}}$ denotes sub-problem $\widetilde{\text{(P.1)}}$ for $\mathbf{q}_1 \in \mathcal{I}_b^1$, where constraint C7b replaces C7.

The proposed SCA algorithm to solve (P.1) is omitted due to space limitation, but is similar to **Algorithm 1**, where the convex approximations $\widetilde{\text{(P.1.a)}}$ and $\widetilde{\text{(P.1.b)}}$ are solved in parallel using CVXPY [16], with precision $\epsilon_1 = \epsilon_0$. The algorithm converges to a local optimum of the upper bound on sub-problem (P.1) entailing computational complexity $\mathcal{O}(2M_1(N+2)^{3.5})$, where M_1 is the required number of iterations [17].

Algorithm 2 Alternating Optimization Algorithm

- 1: Set initial formation $\mathcal{Q}^{(1)} = \{\mathbf{q}_0^{(1)}, \mathbf{q}_1^{(1)}, \mathbf{q}_2^{(1)}\}$, initial communication transmit powers $\mathcal{P}^{(1)} = \{\mathbf{P}_{\text{com},0}^{(1)}, \mathbf{P}_{\text{com},1}^{(1)}, \mathbf{P}_{\text{com},2}^{(1)}\}$, iteration index $m = 1$, and error tolerance $0 < \epsilon_2 \ll 1$.
 - 2: **repeat**
 - 3: Set $m = m + 1$
 - 4: Determine $\overline{\sigma}_h(\mathbf{q}_0, \mathbf{q}_1^{(m-1)}, \mathbf{q}_2^{(m-1)})$ and set $\mathbf{q}_0^{(m)} = \mathbf{q}_0$ and $\mathbf{P}_{\text{com},0}^{(m)} = \mathbf{P}_{\text{com},0}$ after solving (P.0) for fixed $\{\mathbf{q}_1^{(m-1)}, \mathbf{q}_2^{(m-1)}, \mathbf{P}_{\text{com},1}^{(m-1)}, \mathbf{P}_{\text{com},2}^{(m-1)}\}$ using **Algorithm 1**
 - 5: Determine $\overline{\sigma}_h(\mathbf{q}_0^{(m-1)}, \mathbf{q}_1, \mathbf{q}_2^{(m-1)})$ and set $\mathbf{q}_1^{(m)} = \mathbf{q}_1$ and $\mathbf{P}_{\text{com},1}^{(m)} = \mathbf{P}_{\text{com},1}$ after solving (P.1) for fixed $\{\mathbf{q}_0^{(m-1)}, \mathbf{q}_2^{(m-1)}, \mathbf{P}_{\text{com},0}^{(m-1)}, \mathbf{P}_{\text{com},2}^{(m-1)}\}$ using SCA
 - 6: Determine $\overline{\sigma}_h(\mathbf{q}_0^{(m-1)}, \mathbf{q}_1^{(m-1)}, \mathbf{q}_2)$ and set $\mathbf{q}_2^{(m)} = \mathbf{q}_2$ and $\mathbf{P}_{\text{com},2}^{(m)} = \mathbf{P}_{\text{com},2}$ after solving (P.2) for fixed $\{\mathbf{q}_0^{(m-1)}, \mathbf{q}_1^{(m-1)}, \mathbf{P}_{\text{com},0}^{(m-1)}, \mathbf{P}_{\text{com},1}^{(m-1)}\}$ using SCA
 - 7: **until** $\left| \frac{\overline{\sigma}_h(\mathbf{q}_0^{(m)}, \mathbf{q}_1^{(m)}, \mathbf{q}_2^{(m)}) - \overline{\sigma}_h(\mathbf{q}_0^{(m-1)}, \mathbf{q}_1^{(m-1)}, \mathbf{q}_2^{(m-1)})}{\overline{\sigma}_h(\mathbf{q}_0^{(m)}, \mathbf{q}_1^{(m)}, \mathbf{q}_2^{(m)})} \right| \leq \epsilon_2$
 - 8: **return** solution $\{\mathcal{Q}, \mathcal{P}\} = \{\mathbf{q}_0^{(m)}, \mathbf{q}_1^{(m)}, \mathbf{q}_2^{(m)}, \mathbf{P}_{\text{com},0}^{(m)}, \mathbf{P}_{\text{com},1}^{(m)}, \mathbf{P}_{\text{com},2}^{(m)}\}$
-

C. Solution to Problem (P)

To solve problem (P), we use AO by solving sub-problems (P.0), (P.1), and (P.2) iteratively, see Figure 2. In **Algorithm 2**, we summarize all steps used to solve problem (P). **Algorithm 2** converges to a local optimum of the worst-case height error, $\overline{\sigma}_h$, with time complexity $\mathcal{O}(M_2(2M_1 + M_0)(N+2)^{3.5})$, where M_2 is the required number of iterations [17].

V. SIMULATION RESULTS

This section presents simulation results for **Algorithm 2**, using parameters from Table I, unless stated otherwise. To evaluate performance, we adopt the next benchmark schemes:

TABLE I: System parameters [9], [10], [14].

Parameter	Value	Parameter	Value	Parameter	Value
N	80	$P_{\text{com}}^{\text{max}}$	9 dB	λ	0.12 m
δ_t	1 s	$E_{\text{com}}^{\text{max}}$	600 J	$\tau_p \times \text{PRF}$	10^{-4}
z_{min}	1 m	$R_{\text{min},0}$	10 Mbit/s	θ_d	45°
z_{max}	100 m	$R_{\text{min},1}$	17 Mbit/s	T_{sys}	400 K
$h_{\text{amb}}^{\text{min}}$	1.2 m	$R_{\text{min},2}$	1 Mbit/s	B_{Rg}	3 GHz
$h_{\text{amb}}^{\text{max}}$	2.2 m	$B_{c,k}, \forall k$	1 GHz	F	5 dB
x_t	20 m	γ	18.75 dB	L	6 dB
g_x	70 m	$\gamma_{\text{Rg}}^{\text{min}}$	0.8	f_0	2.5 GHz
g_y	150 m	$\gamma_{\text{SNR}}^{\text{min}}$	0.8	$\epsilon_0 = \epsilon_1 = \epsilon_2$	10^{-2}
g_z	25 m	γ_{other}	0.6	$\theta_{3\text{dB}}$	30°
d_{min}	2 m	σ_0	-3 dB	θ_{min}	37.24°
S_{min}	55 m	P_t	23 dBm	θ_{max}	48.7°
v_y	4.3 m/s	$G_r = G_t$	5 dBi	n_L	4

- **Benchmark scheme 1:** Here, a single-baseline UAV-InSAR system consisting only of U_0 and U_1 is considered [11]. The upper bound on the height error σ_{h_1} is minimized based on a two-step AO algorithm.
- **Benchmark scheme 2:** In this scheme, we fix the position of the master UAV at $\mathbf{q}_0 = \mathbf{q}_0^{\text{fixed}}$, which is feasible for (P), and optimize the remaining variables.
- **Benchmark scheme 3:** Here, we apply a static and constant communication power allocation (i.e., $P_{\text{com},k}[n] = \frac{E_{\text{com}}^{\text{max}}}{N}, \forall n, \forall k$), and optimize the remaining variables.

In Figure 3, we present the height error of the final DEM σ_h and its upper bound $\bar{\sigma}_h$ versus the minimum HoA, $h_{\text{amb}}^{\text{min}}$. The figure shows that the sensing accuracy degrades with stricter requirements on the minimum HoA, which is due to the relation between the HoA and the height error, see (13). We note that the tightness of the upper bound on the height error in (18) increases with stricter sensing requirements, i.e., if $\gamma_{\text{SNR}}^{\text{min}} \gamma_{\text{Rg}}^{\text{min}} \gamma_{\text{other}} \rightarrow 1$, then $\sigma_h \rightarrow \bar{\sigma}_h$. Nevertheless, Figure 3 reveals that even for system parameters, for which the upper bound is not tight, it is a useful metric for optimization. In fact, the proposed scheme consistently achieves a gain of at least 39.3% compared to benchmark scheme 1. This gain is due to averaging the height error, which improves the sensing accuracy and highlights the importance of using multiple UAVs for acquisition. Additionally, optimizing the UAV formation and the communication power allows the proposed solution to outperform both benchmark schemes 2 and 3, with a gain that varies with the HoA. For instance, for $h_{\text{amb}}^{\text{min}} = 1.2$ m, respective gains of 20.5% and 12.5% are observed.

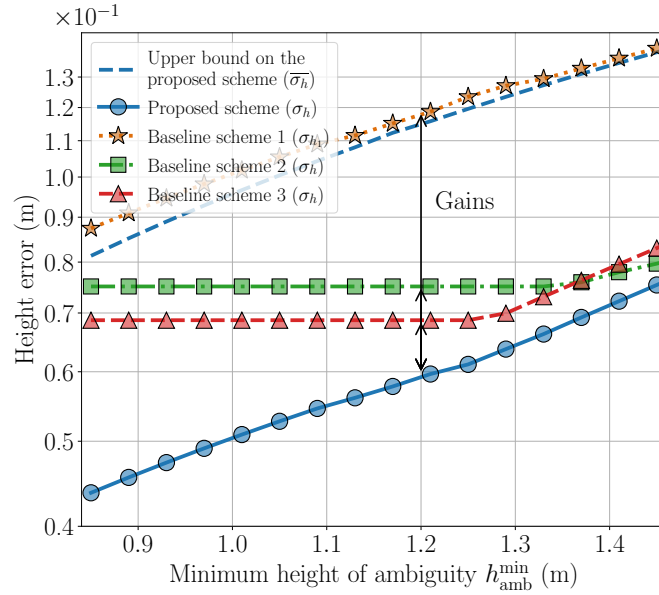


Fig. 3: Height error of the final DEM, σ_h , and its upper bound, $\overline{\sigma}_h$, versus the minimum HoA, h_{amb}^{\min} , for $\mathbf{q}_0^{\text{fixed}} = (-44.2, 64.2)^T$ m.

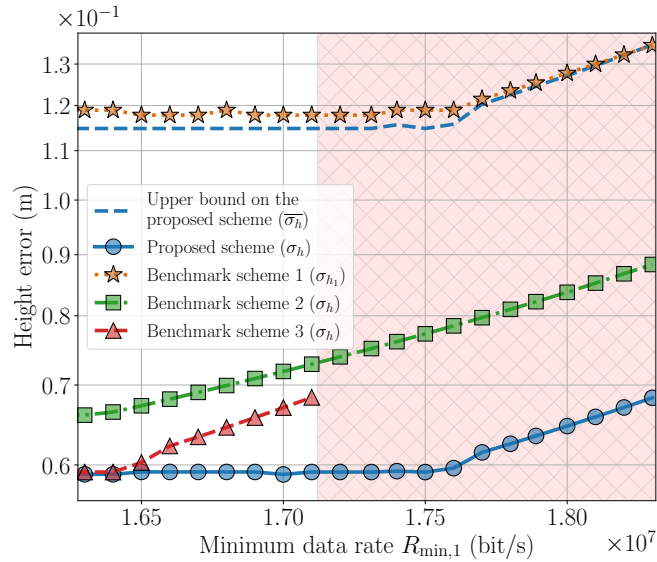


Fig. 4: Height error of the final DEM, σ_h , and its upper bound, $\overline{\sigma}_h$, versus the minimum data rate $R_{\text{min},1}$, for $\mathbf{q}_0^{\text{fixed}} = (-42.5, 62.5)^T$ m.

Figure 4 depicts the final height error and its upper bound versus the minimum data rate of U_1 . The figure shows that higher data rate requirements lead to worse accuracy. This can be explained by U_1 's extended range when lower data rates are sufficient. In contrast, increasing the data rate requirement limits the U_1 -GS distance, which affects the perpendicular baseline and increases the height estimation error.

Furthermore, Figure 4 highlights the need to properly allocate the communication power to ensure real-time data offloading to the GS. A static power allocation, as in benchmark scheme 3, negatively affects the height error and eventually leads to infeasibility of problem (P) starting from $R_{\min,1} = 17.1$ Mbit/s, indicated by the red colored region in Figure 4. Figure 4 confirms that the proposed scheme outperforms all benchmark schemes.

VI. CONCLUSION

In this work, we studied a dual-baseline UAV-based InSAR system using a swarm of three drones to generate two independent DEMs of a target area. The final DEM is obtained with a weighted averaging technique, improving sensing precision. We proposed a low-complexity algorithm that minimizes an upper bound on the height estimation error of the final DEM by jointly optimizing the UAV formation and communication power allocation, while meeting sensing and communication constraints. Simulation results showed that the proposed scheme significantly improves sensing accuracy compared to single-baseline systems and other benchmark schemes.

APPENDIX A

BI-STATIC SNR APPROXIMATION

In this appendix, we provide the detailed steps for deriving the bi-static SNR approximation in (9). To this end, we start with the bi-static radar SNR expression for distributed targets, denoted by SNR_r and given by [13]:

$$\text{SNR}_r = \frac{\sigma_0 A_{\text{res}} P_t G_t G_r \lambda^2}{(4\pi)^3 R_{\text{Tx}}^2 R_{\text{Rx}}^2 k_b B_{\text{noise}} T_{\text{sys}} FL}, \quad (22)$$

where R_{Tx} and R_{Rx} represent the radar transmit and receive slant ranges, respectively, A_{res} is the size of one resolution cell, i.e., the size of the smallest area the SAR system can distinguish, B_{noise} is the effective noise bandwidth, and L denotes the total radar losses. After coherent integration of the radar signal to form the SAR image, the radar SNR is improved by a factor N_{proc} as follows:

$$\text{SNR} = \text{SNR}_r N_{\text{proc}} = \text{SNR}_r N_{\text{pulse}} N_a, \quad (23)$$

where N_{pulse} is the number of samples per pulse and N_a is the number of samples within the synthetic aperture length, which is denoted by L_a . Note that $N_{\text{pulse}} = \tau_p B_{\text{Rg}} \approx \tau_p B_{\text{noise}}$ and $N_a = \frac{L_a \text{PRF}}{v_y}$. Thus, the image SNR can be written as:

$$\text{SNR} = \frac{\sigma_0 A_{\text{res}} P_t G_t G_r \lambda^2 \tau_p \text{PRF} L_a}{(4\pi)^3 R_{\text{Tx}}^2 R_{\text{Rx}}^2 v_y k_b T_{\text{sys}} FL}. \quad (24)$$

The SNR expression depends on the resolution cell size A_{res} , which is related to the range and azimuth resolutions, denoted by δ_r and δ_a , respectively. For a mono-static system with slant range R_{Tx} and incidence angle θ , $A_{\text{res}} = \delta_r \delta_a = \frac{\lambda R_{\text{Tx}} c}{4 B_{\text{Rg}} L_a \sin(\theta)}$ leads to the expression in (8) [10]. However, calculating A_{res} for the bi-static case is more complex. According to [18], in this case, the ground range resolution is given by:

$$\delta_r = \frac{c}{B_{\text{Rg}} (\sin(\theta_{\text{Tx}}) + \sin(\theta_{\text{Rx}}))}, \quad (25)$$

where θ_{Tx} and θ_{Rx} denote the transmit and receive incidence angles, respectively. Furthermore, the azimuth resolution is given by:

$$\delta_a = l \frac{R_{\text{Rx}}}{R_{\text{Tx}} + R_{\text{Rx}}}. \quad (26)$$

In the case of across-track interferometry applications, since a lower bound is imposed on the baseline decorrelation by constraint C7, the bi-static angle $\Delta\theta = |\theta_{\text{Tx}} - \theta_{\text{Rx}}|$ is relatively small (i.e., on the order of few degrees). Thus, the range resolution can be approximated by $\delta_r \approx \frac{c}{2 B_{\text{Rg}} \sin(\theta_{\text{Tx}})}$ and $\sigma_0(\theta_{\text{Rx}}) \approx \sigma_0(\underbrace{\theta_{\text{Tx}}}_{\text{fixed angle}}) = \sigma_0$. Based on the bi-static effective range $R_{\text{eff}} = \frac{R_{\text{Rx}} + R_{\text{Tx}}}{2}$, we approximate the azimuth resolution as:

$$\delta_a \approx \frac{\lambda R_{\text{eff}} R_{\text{Rx}}}{L_a (R_{\text{Tx}} + R_{\text{Rx}})}, \quad (27)$$

which leads to the following approximation of the resolution cell size:

$$A_{\text{res}} = \delta_r \delta_a \approx \frac{\lambda R_{\text{Rx}} c}{4 L_a B_{\text{Rg}} \sin(\theta_{\text{Tx}})}. \quad (28)$$

Finally, the approximated bi-static SNR expression is obtained by inserting (28) in (24).

APPENDIX B

PROOF OF PROPOSITION 1

It can be shown that σ_{Φ_k} is monotonically decreasing w.r.t. the total coherence γ_k . Therefore, given the worst-case coherence value $\mathcal{A} = \gamma_{\text{Rg}}^{\min} \gamma_{\text{SNR}}^{\min} \gamma_{\text{other}}$, the following inequality holds:

$$\sigma_{\Phi_k}(\mathbf{q}_0, \mathbf{q}_k) \leq \frac{1}{\mathcal{A}} \sqrt{\frac{1 - \mathcal{A}^2}{2n_L}}, \forall k \in \{1, 2\}. \quad (29)$$

Based on (13), (17), and (29), we construct an upper bound on the height error σ_{h_k} of interferometric pair (U_0, U_k) as follows:

$$\sigma_{h_k}(\mathbf{q}_0, \mathbf{q}_k) \leq \frac{\lambda r_0(\mathbf{q}_0) \sin(\theta_0)}{2\pi b_{\perp, k}(\mathbf{q}_k) \mathcal{A}} \sqrt{\frac{1 - \mathcal{A}^2}{2n_L}}, \forall k \in \{1, 2\}. \quad (30)$$

The proof is concluded by inserting the upper bound (30) into the expression for the height error of the final DEM, given in (15).

APPENDIX C

PROOF OF PROPOSITION 2

Let function $f(x) = \frac{1}{B_p} \left[\frac{2+B_p}{1+x} - \frac{2-B_p}{1+\frac{1}{x}} \right]$ such that $f(\mathcal{X}(\mathbf{q}_k))$ represents the baseline decorrelation. Note that $\forall \mathbf{q}_k, 0 \leq \mathcal{X}(\mathbf{q}_k) \leq 2$, therefore, we focus on function f in the domain $[0, 2]$. It can be shown that function f is a decreasing and invertible function such that:

$$f^{-1}(x) = h(x) = \frac{B_p x - 2 - B_p}{B_p - 2 - x B_p}. \quad (31)$$

Therefore, constraint C7 is equivalent to the following constraint:

$$C7 : f(\mathcal{X}(\mathbf{q}_k)) \geq \gamma_{\text{Rg}}^{\min} \iff \mathcal{X}(\mathbf{q}_k) \leq h(\gamma_{\text{Rg}}^{\min}). \quad (32)$$

Based on (11) and (32), constraint C7 is equivalent to the following constraints:

$$\begin{cases} \text{C7a} : \sin(\theta_k(\mathbf{q}_k)) \geq \frac{2 - h(\gamma_{\text{Rg}}^{\min})}{h(\gamma_{\text{Rg}}^{\min})} \sin(\theta_0), \text{ if } \mathbf{q}_k \in \mathcal{I}_a^k, \\ \text{C7b} : \sin(\theta_k(\mathbf{q}_k)) \leq \frac{h(\gamma_{\text{Rg}}^{\min})}{2 - h(\gamma_{\text{Rg}}^{\min})} \sin(\theta_0), \text{ if } \mathbf{q}_k \in \mathcal{I}_b^k. \end{cases} \quad (33)$$

Note that constraints C7a and C7b are in general non-convex, however, knowing that $0 \leq \theta_k(\mathbf{q}_k) \leq \frac{\pi}{2}, \forall \mathbf{q}_k, \forall k$, then we can apply increasing functions arcsin and tan to (33), which results in the following equivalent convex constraints:

$$\begin{cases} \text{C7a} : \frac{x_t - x_k}{z_k} \geq \tan \left(\arcsin \left(\frac{(2 - h(\gamma_{\text{Rg}}^{\min})) \sin(\theta_0)}{h(\gamma_{\text{Rg}}^{\min})} \right) \right), \text{ if } \mathbf{q}_k \in \mathcal{I}_a^k, \forall k, \\ \text{C7b} : \frac{x_t - x_k}{z_k} \leq \tan \left(\arcsin \left(\frac{h(\gamma_{\text{Rg}}^{\min}) \sin(\theta_0)}{2 - h(\gamma_{\text{Rg}}^{\min})} \right) \right), \text{ if } \mathbf{q}_k \in \mathcal{I}_b^k, \forall k. \end{cases} \quad (34)$$

REFERENCES

- [1] G. Pajares, "Overview and current status of remote sensing applications based on unmanned aerial vehicles (UAVs)," *Photogramm. Engineer. Remote Sens.*, vol. 81, no. 4, pp. 281–330, 2015.
- [2] I. Ullmann *et al.*, "Towards detecting climate change effects with UAV-borne imaging radars," *IEEE J. Microw.*, 2024, early access.
- [3] H. Ren *et al.*, "Swarm UAV SAR for 3-D imaging: System analysis and sensing matrix design," *IEEE Trans. Geosci. Remote Sens.*, vol. 60, pp. 1–16, 2022.
- [4] M.-A. Lahmeri *et al.*, "Robust trajectory and resource optimization for communication-assisted UAV SAR sensing," *IEEE Open J. Commun. Soc.*, vol. 5, pp. 3212–3228, 2024.
- [5] —, "Trajectory and resource optimization for UAV synthetic aperture radar," in *Proc. IEEE Global Commun. Conf.*, 2022, pp. 897–903.
- [6] Z. Sun *et al.*, "Trajectory optimization for maneuvering platform bistatic SAR with geosynchronous illuminator," *IEEE Trans. Geosci. Remote Sens.*, vol. 62, pp. 1–15, 2024.
- [7] A. Grathwohl *et al.*, "Detection of objects below uneven surfaces with a UAV-based GPSAR," *IEEE Trans. Geosci. Remote Sens.*, vol. 61, pp. 1–13, 2023.

- [8] P. Rosen *et al.*, “Synthetic aperture radar interferometry,” *Proc. IEEE*, vol. 88, no. 3, pp. 333–382, 2000.
- [9] M. Martone *et al.*, “Coherence evaluation of TanDEM-X interferometric data,” *ISPRS J. Photogramm. Remote Sens.*, vol. 73, pp. 21–29, 2012.
- [10] G. Krieger *et al.*, “TanDEM-X: A satellite formation for high-resolution SAR interferometry,” *IEEE Trans. Geosci. Remote Sens.*, vol. 45, no. 11, pp. 3317–3341, 2007.
- [11] M.-A. Lahmeri *et al.*, “UAV formation optimization for communication-assisted InSAR sensing,” in *Proc. IEEE Int. Conf. Commun. (ICC)*, 2024, pp. 3913–3918.
- [12] A. Gruber *et al.*, “The TanDEM-X DEM mosaicking: Fusion of multiple acquisitions using InSAR quality parameters,” *IEEE J. Sel. Top. Appl. Earth Obs. Remote Sens.*, vol. 9, no. 3, pp. 1047–1057, 2016.
- [13] M. I. Skolnik *et al.*, *Introduction to Radar Systems*. McGraw-hill New York, 1980, vol. 3.
- [14] V. Mustieles-Perez *et al.*, “New insights into wideband synthetic aperture radar interferometry,” *IEEE Geosci. Remote Sens. Lett.*, vol. 21, pp. 1–5, 2024.
- [15] J. Mairal, “Optimization with first-order surrogate functions.” PMLR, 2013, pp. 783–791.
- [16] S. Diamond and S. Boyd, “CVXPY: A python-embedded modeling language for convex optimization,” *J. Mach. Learn. Res.*, vol. 17, no. 83, pp. 1–5, 2016.
- [17] S. Boyd and L. Vandenberghe, *Convex Optimization*. Cambridge University Press, 2004.
- [18] M. Cherniakov, *Bistatic Radar: Emerging Technology*. John Wiley & Sons, 2008.